Wafer-level-integrated vertical-waveguide sub-diffraction-limited color splitters

S. Kang[1], M. Benelajla[3,4], R. Mac Ciamain[1], F. Ali[1,2], A. Papadopoulou[1,2], O. Shramkova[1], L. Witters[1], J. De Vos[1], P.E. Malinowski[1], P. Heremans[1,2],N. Le Thomas[3,4], B. Figeys[1], R. Gehlhaar[1] and J. Genoe[1,2]

[1]Imec, Kapeldreef 75, 3001 Leuven, Belgium, email: jan.genoe@imec.be
[2]KU Leuven, ESAT Department, Kasteelpark Arenberg 10 - bus 2440, 3001 Leuven, Belgium
[3]Photonics Research Group, INTEC Department, Ghent University-imec, Technologiepark-Zwijnaarde 126, 9052 Ghent, Belgium
[4]Center for Nano- and Biophotonics, Ghent University, Technologiepark Zwijnaarde 15, 9052 Ghent, Belgium

***Abstract* —** We demonstrate a new technology for splitting colors with sub-micron resolution using standard backend processing on 300 mm wafers. The color splitting is tunable via the geometry and can be designed to correspond to the color sensitivity of the human eye. The technology can result in: higher signal-to-noise ratio, better color quality and enhanced resolution for high-end cameras.

I. INTRODUCTION

CMOS image sensor (CIS) scaling has reached pixel sizes as small as 0.56 µm [1], reaching the Abbe limit. However, high-quality cameras typically use larger pixels because the signal that can be captured on extremely small pixels is limited, resulting in lower SNR. Some of the main limitations are posed by the Bayer color filters: (1) they absorb a substantial amount of light and hence reduce the SNR, (2) they limit the actual image resolution, and (3) being chemically engineered, combinations of absorption characteristics and high-resolution patterning capabilities are limited. To improve this situation, color splitting has been proposed, first at 1.4 µm spatial resolution [2], and subsequently at 0.8 µm [3]. These prior-art diffraction-based approaches solve the absorption disadvantage of color filters, but they do not improve image resolution beyond the Abbe limit. In this work, we propose a fundamentally different way to split colors: not by diffraction, but by the use of the beating pattern between a symmetric and an antisymmetric mode in a multimode waveguide. With this method, we show that we can faithfully split colors within a sub-micron pixel.

II. PRINCIPLE OF COLOR SPLITTING

Figure 1 is a 3D sketch of an array of color splitters according to our implementation, and Fig. 2 shows a cross-section. Each splitter consists of a vertical waveguide (with rectangular cross-section) having a tapered section at the top that acts as an entrance funnel for incident light. The focal plane of the imager objective is positioned at the entrance of these tapered light funnels. Each tapered input has a diffraction-limited size (e.g. $(0.8\,\mu m)^2$), defined by the numerical aperture of the camera lens. The tapered waveguide section forms an adiabatic funnel for the incident (white) light, that squeezes the light into a single mode at the taper exit. This taper exit feeds the light asymmetrically into the straight rectangular section of the waveguide below, ensuring the transformation of the single mode at the exit of the taper into a symmetric and antisymmetric mode in the rectangular waveguide. The propagation speed between the symmetric and antisymmetric mode is different for each wavelength. We design the dimensions of the waveguides such that a desired color composition difference is attained between a "left" and "right" exit. This will be elaborated in section IV.

III. FABRICATION OF THE OPTICAL STACK

For the fabrication of the optical stack, we have selected Si_3N_4 waveguides in a SiO_2 matrix. Other material systems, with higher refractive index contrast, are possible as well, but we opted for the well-established, standard Si_3N_4 / SiO_2 material system. Fig. 2 shows the process stack sequence on a silicon 300 mm wafer. The 6-µm tall waveguides are processed as three layers of 2 µm each, by repeating three times the following steps: SiCN / SiO_2 deposition, trench patterning in SiO_2, trench filling with conformal deposition of SiN, planarization. The sidewall profiles of the trench etch have been optimized to match the desired profiles, established from Finite Difference Time Domain (FDTD) simulation. Note that the 4-µm straight waveguide is formed in two subsequent iterations: this was done to comply with good practices regarding etch-aspect-ratio and stress compensation.

The optical stack of Fig. 2 has been processed on a blank silicon wafer, which in the future can be replaced by a CMOS image sensor wafer. The Si wafer is not transparent in the visible. For the purpose of optical characterization of our bare color splitters, we therefore replaced the Si carrier wafer by a glass carrier after processing of the splitters. To that end (see Fig. 3), a glass carrier was bonded to the entrance funnel side of the splitters and subsequently the Si wafer was removed by grinding and etching. Furthermore, at specific places in the test vehicle, we have introduced 50 nm-thick TiN reflective layers at both the top and the bottom of the waveguide layers (as shown on Fig. 3). At the top, the TiN is covering unused space between input tapers. At the bottom, TiN covers either the left half or the right half of the waveguide exits, to purposely occlude the left or right light exits: in this way, it is readily possible to visualize the color splitting of white light by inspecting the light at the exits of the waveguides. A TEM cross-section of the transferred components on a glass

substrate is shown in Fig. 4 (some waveguide exits are half occluded by TiN, some not), the full wafer on glass is shown in Fig. 5.

IV. Optical characterisation

A. White light illumination

The optical stack as shown in Fig. 3 and 4 has first been characterized under plane-wave white-light illumination and RGB camera detection at 100× magnification. Figure 6 shows an area on the wafer with alternating 5×5 left-side-open-aperture and 5×5 right-side-open-aperture waveguides, for a particular waveguide design that is designed to split off blue light from the rest of the spectrum. Fig. 7 sketches the expected response to white light: the blue wavelength range is collected at the left exit, whereas the remaining wavelength range is collected at the right exit. The corresponding colors are visible in the measurement of Fig. 6.

On the processed 300 mm wafer, we have designed a broad range of waveguides. We have varied following parameters: (1) waveguide short axis, (2) waveguide long axis, (3) taper exit offset, (4) taper entrance geometry, (5) various alignment variations of taper on rectangular waveguide. In Fig. 8, we show measurements of a small subset of variations (1) and (2) under uniform white light illumination, demonstrating how the color transition region at the exit of waveguides (not blocked by TiN) can be designed to move from between blue and green to between green and red.

B. Confocal microscopy

A more detailed analysis of a selected single waveguide was performed by focusing blue, green and red laser beams at the input of the optical stack and imaging the output with a diffraction-limited high-numerical-aperture (NA:0.95) microscope objective. Fig. 9 shows the measured exit intensity profiles for each color of the selected waveguide. Fig. 10 shows the intensity profile of the same measurement along the middle of the waveguide. It emerges that the symmetric and antisymmetric modes for the blue and red laser light sum such that the light is dominantly present at the right and left waveguide exit, respectively. Under green laser light, a symmetric propagation mode persists, yielding almost equal left and right detector signals.

V. Color quality

It emerges that the best matching of color splitting with the performance of the cones of the human eye is obtained for splitters designed such that the spectra at the right and left of a waveguide exit plane cross at the same wavelength where the human cone sensitivity curves cross each other. As we have three cones, we need two waveguides, one with a crossing point between blue and green and one with a crossing point between green and red (Fig. 11 and 12). We designed two waveguide stacks (table I) according to these specifications, that match human cone performance. Importantly, it can also be seen that the total output light from each waveguide (curves "both" in the Figs) is more than 90 % in the wavelength range 400-700 nm, which is far superior to color filters.

Finally, we performed a detailed study of the color quality in comparison with an online database [4] of Bayer color filters in high-end full-frame cameras. We used the methodology defined by Vora *et al*. [5]. Typically, in these assessments, a standard observer (as specified in CIE 1931 2°), is used, as marked by the blue dot in Fig. 13. In order to avoid the dedicated tweaking of the color response to a single observer, we extended the color observers to a broad database of people among all races, continents and ages [6]. The overall color quality also depends on the detector sensitivity that is present below the optical stack. The read-out optimization goes beyond the scope of this work, but we made an assessment with three detectors of Fig 14: two commercial CIS detectors and as an alternative a CMOS compatible broadband thin-film photodetector (275-nm-thick $CsPbI_2Br$ perovskite detector deposited in our lab), each extended with a commercial UV filter (PixelTex @420 nm). Fig. 13 shows that embodiment of the color splitter in state-of-the-art CIS already provides color quality on par with most high-end cameras, whereas future image sensors (or IR filtering @650 nm) will provide further CIS color quality improvement.

VI. Summary and Outlook

In a successfully integrated vertical-waveguide array, we demonstrated sub-diffraction limited color splitting to match the human eye color sensitivity space with a Vora value > 95 %. These optical elements offer a wide range of tunability by design to comply with Si-based or emerging thin-film CMOS imager technology. With its proven sub-micron color separation, it enables further scaling of high-resolution imagers with the ultimate target to detect every incident photon.

Acknowledgment

We acknowledge the financial support from the Fund for Scientific Research Flanders (FWO) under Project number S004322N (GigaPixel).

References

[1] S. Park *et al.*, "A 64Mpixel CMOS Image Sensor with 0.56μm Unit Pixels Separated by Front Deep-Trench Isolation," in *2022 IEEE International Solid- State Circuits Conference (ISSCC)*, Feb. 2022, paper 5.8

[2] S. Nishiwaki *et al.* "Efficient colour splitters for high-pixel-density image sensors". Nat. Photonics 7, 240 (2013)

[3] S. Yun *et al.* "Highly Efficient Color Separation and Focusing in the Sub-micron CMOS Image Sensor.", IEDM 2021, paper 30.1.1

[4] https://zenodo.org/communities/colour-science-datasets

[5] P.L. Vora and H.J. Trussell, "Measure of goodness of a set of color-scanning filters," J.Opt.Soc.Am. A **10**, 1499 (1993)

[6] H. Xie and M.D. Fairchild, "The Luther Condition for All: Evaluating Colorimetric Camera Design for Personalized Color Imaging," in Proc. AIC 2022 Sensing Colour, Toronto, Canada, Jun. 2022.

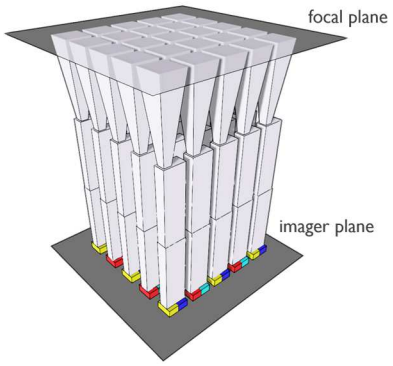

Fig. 1. 3D visualization of the vertical waveguide array for color splitting for BY-CR imaging.

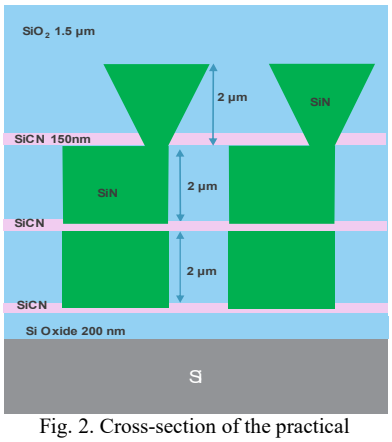

Fig. 2. Cross-section of the practical implementation of the concept

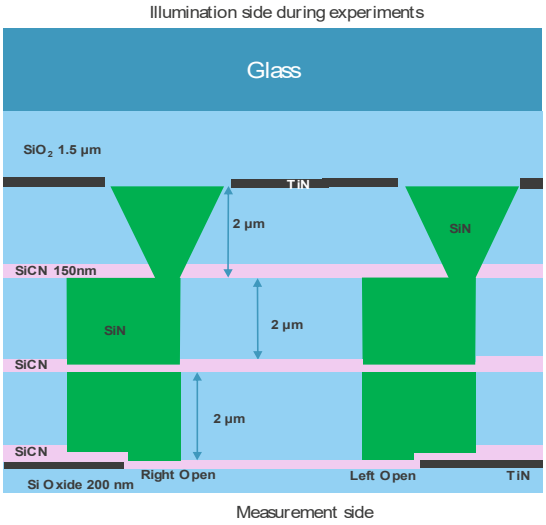

Fig. 3. Schematics of processed structures, bonded to carrier glass, with TiN blocking half of exits for characterization purposes.

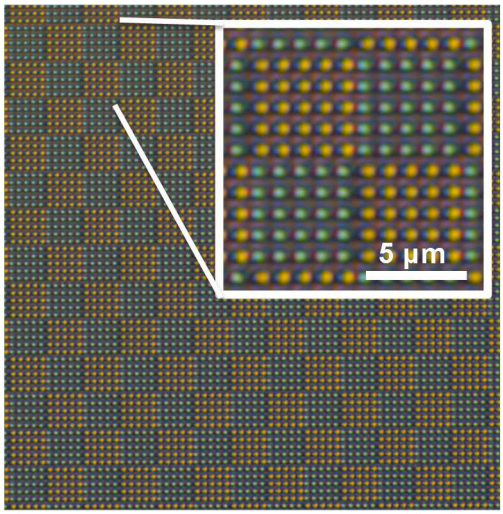

Fig. 6. RGB camera measurement (100× magnification) of a structure of 620nm × 250nm waveguides with alternating 5 left-side-open-aperture and 5 right-side-open-aperture (the others being occluded by TiN) waveguides at a 1-micron pitch.

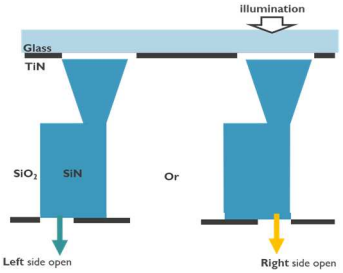

Fig. 7. Visualization of the measurement in Fig 6 on a part of the wafer with alternating blocking layers. Yellow light exits at the right part of the waveguide, whereas the blue exits at the left. The wafer is illuminated using plane wave white light.

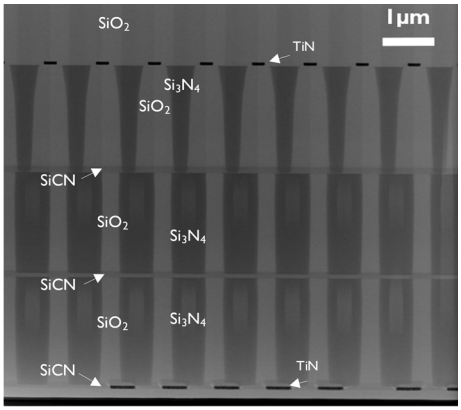

Fig. 4. TEM X-section comprising (left) two waveguides with both-sides aperture exits, five waveguides with right-side aperture exits and (right) two waveguides with left-side aperture exits.

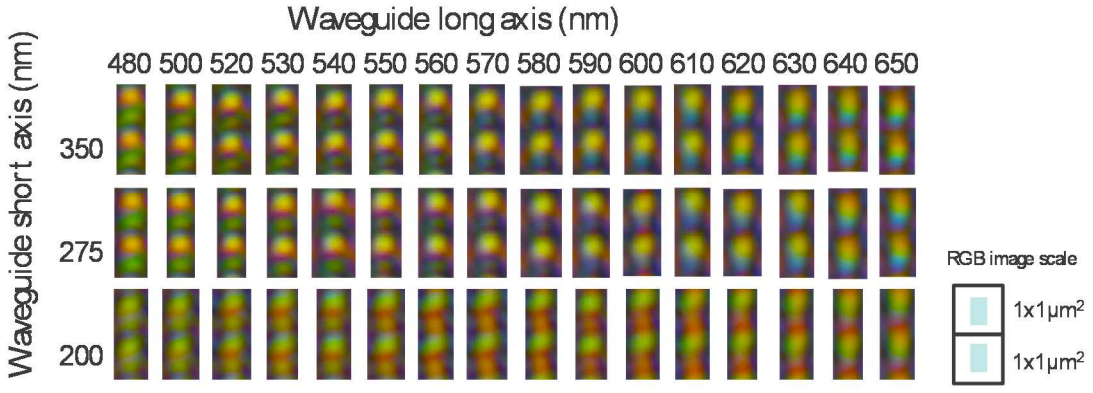

Fig. 8. RGB camera (3.45 µm pixel size) measurement (under 100× magnification) of the output of two waveguides under uniform white light illumination. The huge design parameter space is pinpointed from the variations of only the long waveguide and the short waveguide axes variations. Other variations, such as taper exit offset, waveguide length taper width and taper spacing are not shown. The square rectangles show the scale and the waveguide relative position.

Fig. 5. Photo of the 300 mm wafer bonded on glass.

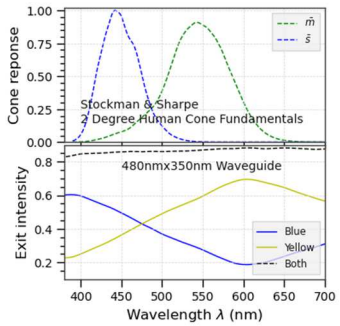

Fig. 11. (Top) standard CIE observer blue and green human eye response with crossing point at 480 nm. (bottom) Lumerical FDTD simulation of the left and right detector signal below a 480 nm × 350 nm waveguide.

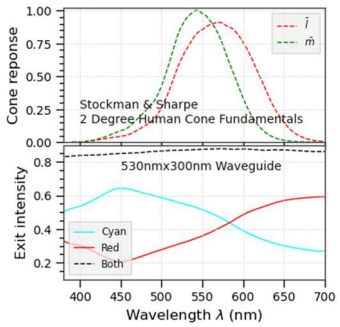

Fig. 12. (Top) standard CIE observer red and green human eye response with crossing point at 580 nm. (bottom) Lumerical FDTD simulation of the left and right detector signal below a 530 nm × 300 nm waveguide.

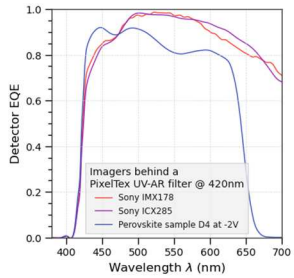

Fig. 14. Detector EQE used in the Vora value assessment of Fig 13

Unit cell		800 nm × 800 nm
Taper top		700 nm × 700 nm
Taper bottom		250 nm × 250 nm
Taper length		2 µm
Waveguide length		4 µm
Waveguide	Fig 11	480 nm × 350 nm
	Fig 12	530 nm × 300 nm
Taper exit shift	Fig 11	115 nm
	Fig 12	140 nm

Table I: Lumerical FDTD simulation parameters used in Fig. 11 and Fig. 12

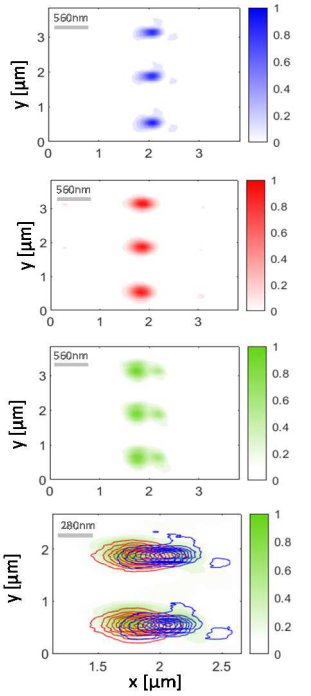

Fig. 9. Measured confocal microscope intensity (NA:0.95) below two 560 nm × 300 nm waveguide exits under blue (450 nm) (top), red (632 nm) and green (532 nm) laser illumination (NA:0.45). The bottom graph superimposes the 3 upper graphs.

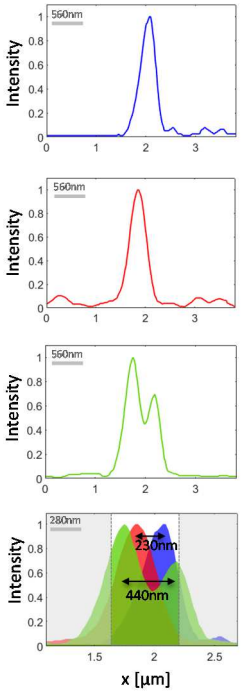

Fig. 10 Optical output intensity measured along the central line in Fig.9. The spatial separation between both modes is clearly visible.

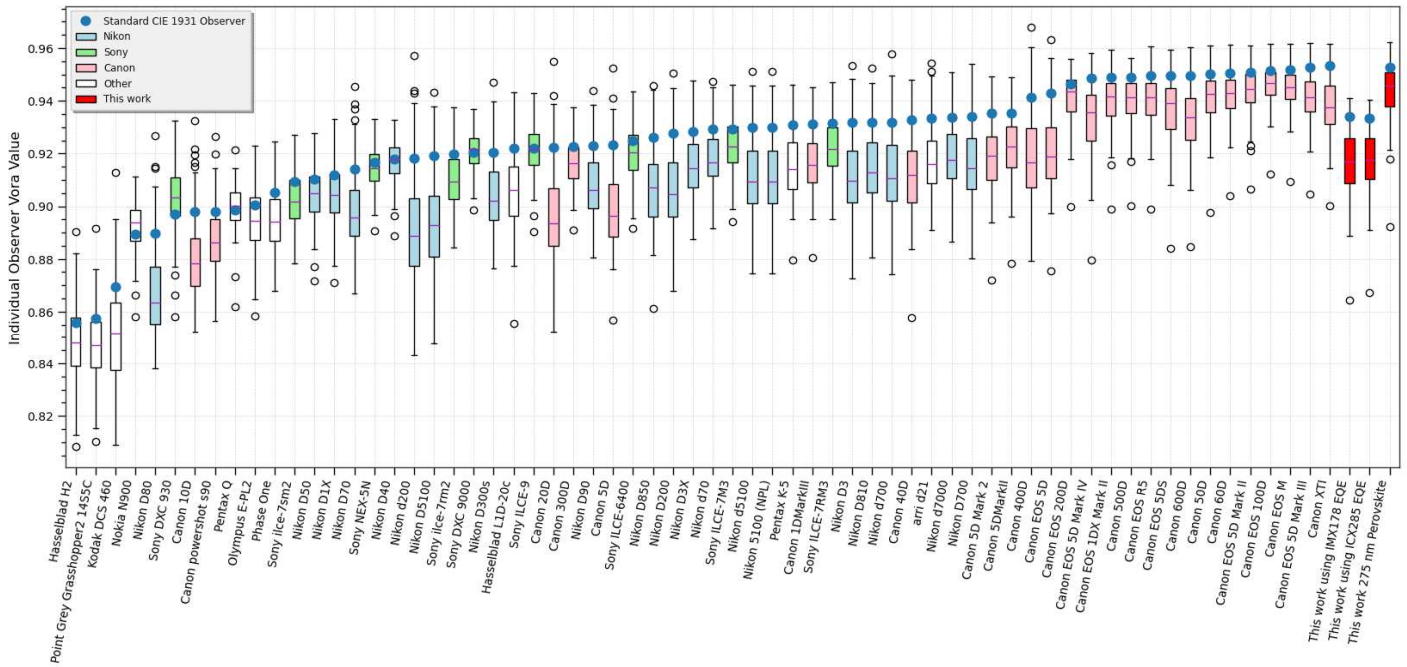

Fig. 13. Vora value measurement of color filters of commercial camera's [5]. In order to improve the assessment of the color quality, not only the standard observer (CIE1931) but also a broad statistical distribution of observers of all races and ages is compared [6]. The matching (by design) with the human eye cone crossing points uses the simulations shown in Figs 11 and 12. Please note that the overall color quality assessment will be even higher than the reported Vora measures as the waveguides collect all incident phonons, in contrast with color filters, which results in an improved SNR of our color splitter over color filters.